*Highlights (for review)

Highlights

- MIS 19 was marked by 5000-year cycles of drying and cooling events in SW Iberia
- These events indicate low latitude-forced northward deflection of the westerlies
- During MIS 19c these events were coeval with warm waters in the subtropical gyre
- These successive air-sea decoupling could contribute to the progressive ice growth
- This work challenges the similar duration of MIS 19c and the Holocene

Tropically-driven climate shifts in southwestern Europe during MIS 19, a low eccentricity interglacial

M.F. Sánchez Goñi[1*], T. Rodrigues[2,3], D. A. Hodell[4], J. M. Polanco-Martínez[5], M. Alonso-García[2,3], I. Hernández-Almeida[6], S. Desprat[1], P. Ferretti[7]

[1]Ecole Pratique des Hautes Etudes, UMR CNRS 5805 EPOC, University of Bordeaux, 33615 Pessac, France

[2] Divisão de Geologia e Georecursos Marinhos, Instituto Português do Mar e da Atmosfera, Rua Alfredo Magalhães Ramalho, 6,1495-006 Lisboa, Portugal

[3] Centro de Ciências do Mar (CCMAR), Universidade do Algarve, Campus de Gambelas, 8005-139 Faro, Portugal

[4] Godwin Laboratory for Palaeoclimate research, Department of Earth Sciences, University of Cambridge, UK

[5] Basque Centre for Climate Change - BC3, 48008 Bilbao, Spain

[6] Institute of Geography & Oeschger Centre for Climate Change Research, University of Bern, 3012 Bern, Switzerland

[7] Consiglio Nazionale delle Ricerche, Istituto per la Dinamica dei Processi Ambientali (CNR-IDPA), Venice I-30123, Italy

* Corresponding author: M.F. Sánchez Goñi, e-mail: mf.sanchezgoni@epoc.u-bordeaux1.fr

Abstract

The relative roles of high- versus low-latitude forcing of millennial-scale climate variability is not well known. Here we show that millennial variability during Marine Isotope Stage (MIS) 19, a period of reduced eccentricity centered at 785 ka and the best analogue to our present interglacial from an astronomical point of view, was related to a nonlinear response to Earth's precession cycle. We present terrestrial-marine climate profiles from the southwestern Iberian margin, a region particularly affected by precession. In contrast to our present interglacial, we show for the first time low latitude-driven 5000-year cycles of drying and cooling in the western Mediterranean region along with warmth in the subtropical gyre related to the fourth harmonic of precession. These cycles indicate repeated intensification of North Atlantic meridional moisture transport that along with decrease in boreal summer insolation triggered ice growth and may contribute to the glacial inception, at ~774 ka. Superimposed on this cyclicity freshwater fluxes during MIS 19ab amplified the cooling events in the North Atlantic leading to glaciation. The discrepancy between the dominant cyclicity observed during the Holocene, 2500-yr, and that of MIS 19, 5000-yr, challenges the similar duration of the two analogue interglacials under natural boundary conditions.

Keywords: MIS 19, southwestern Iberian margin, precession harmonics, low-latitude forcing, westerlies

1. Introduction

Millennial-scale climatic changes have been primarily linked to North Atlantic oceanic and atmospheric processes related to ice-sheet dynamics or ice-shelf instability (Marcott et al., 2011; McAyeal, 1993). Repeated freshwater pulses affected the subpolar North Atlantic vertical convection and deep water formation feeding the Atlantic Meridional Overturning Circulation (AMOC). The latter modulates the net northward heat transfer in the Atlantic, thus influencing the climate at regional and global scales (Ganopolski and Rahmstorf, 2001). However, low latitude variations in the seasonal insolation cycle driven by the 23-kyr precession, and its harmonics at 11 and 5.5-kyr have also been invoked to explain the observed and simulated suborbital changes in Atlantic surface oceanography and monsoonal variability, respectively (Berger et al., 2006; Ruddiman and McIntyre, 1984; Tuenter et al., 2007). These suborbital changes are a pervasive feature throughout the Pleistocene and occurred well before the formation of large ice caps in the Northern Hemisphere (Hernández-Almeida et al., 2012; Weirauch et al., 2008). The reason why low latitudes may lead to millennial-scale changes is the double maximum which characterizes the daily irradiation received by the tropical latitudes over the course of the year (Berger et al., 2006). A direct consequence of this process would be a larger latitudinal thermal gradient and the enhanced transport of warmth and moisture by either atmospheric (westerlies) or oceanic circulation (subtropical gyre) from equatorial to the higher latitudes of the North Atlantic (Berger et al., 2006; Short et al., 1991). Along with the decrease in boreal summer insolation, this process is relevant for understanding the ice ages because it provides the winter moisture necessary for the build-up of ice-sheets (Chapman and Maslin, 1999; Ruddiman and McIntyre, 1984).

It has been shown that the precession-driven millennial cycles that punctuated the last 45,000 years modulate the strength and zonality of the trade winds and tropical SST conditions, and therefore the direct advection of low-latitude surface water heat to the North Atlantic high latitudes, during a time of reduced eccentricity modulation (McIntyre and Molfino, 1996). However, no record of North Atlantic atmospheric circulation is available tracing the cyclicity of the northward heat transfer from low latitudes during periods of weak precession forcing, such as our present interglacial (Yin and Berger, 2011). To examine variations in the westerlies by which the energy is transported into high latitudes away from equatorial regions, we present a record of pollen-derived atmospheric changes for MIS 19 from Site U1385, the Shackleton Site, directly compared with North Atlantic oceanic changes and related episodes of ice growth and decay. This site located at 37°N is ideally suited to examine the precessional signal and that of its harmonics, because the climate of regions below 40°N have a strong precessional rhythm (Ruddiman and McIntyre, 1984), and it is directly affected by the westerlies.

2. Material and Methods

2.1 Present-day environmental setting

Site U1385 or Shackleton site (37°34.285'N, 10°7.562'W, 2578 m depth) was recovered during IODP Expedition 339 "Mediterranean Outflow". The site is located on a spur, the Promontorio dos Principes de Avis, along the continental slope of the southwestern Iberian margin, which is elevated above the abyssal plain and influence of turbidites (Hodell et al., 2013) (Fig. 1). The sedimentary section recovered at Site U1385 (1.5 km-long record) shows hemipelagic continental margin sediments deposited under normal marine conditions with a fully oxygenated water column and average sedimentation rates of 10 cm/ky (Stow et al., 2013). The water depth of Site U1385 places it under the influence of Northeast Atlantic Deep Water today, although it was influenced by southern sourced waters during glacial periods (Shackleton et al., 2000).

The southern Iberian margin is located in the north-eastern edge of the subtropical gyre, under the influence of Eastern North Atlantic central water (ENACW). The surface water column is affected by the Portugal current (PC) which brings cold nutrient-rich water from the northern latitudes and forms the ENACW of subpolar origin (ENACWsp), and by the Azores current (AC) which brings warm water from the Azores front generating the ENACW of subtropical origin (ENACWst) (Ríos et al., 1992). The general distribution of water masses is influenced by the seasonal migration of the Azores anticyclonic cell and its associated large-scale wind pattern.

Climate in the southern Iberian margin is directly affected by the westerlies. During winter the North Atlantic westerlies bring moisture to the Iberian margin, while a high pressure cell develops in the North Atlantic during summer, which generates strong northerly Trade winds inducing coastal upwelling (Fiúza et al., 1982). This seasonality of climate is characterized by mild winters (m: 5-1°C; M: 13-8°C) and hot and dry summers (Pann < 600 mm) (Peinado Lorca and Martínez-Parras, 1987), and lead to the development of a Mediterranean vegetation in the adjacent landmasses dominated by deciduous oak at middle elevation, and evergreen oak, olive tree, *Pistacia*, *Phillyrea* and rockroses (*Cistus*) at lower elevations (Blanco Castro et al., 1997). Experimental studies on the pollen representation of western Iberian vegetation in the sediments of its margin (Naughton et al., 2007) show that marine pollen assemblages give an accurate and integrated image of the regional vegetation occupying the adjacent continent. Present-day Mediterranean and

Atlantic forest communities of Iberia are well discriminated by south and north marine pollen spectra, respectively.

2.2 Site stratigraphy

The stratigraphy of Site U1385 was built upon a combination of chemo-stratigraphic proxies (Hodell et al., 2015). Ca/Ti ratio measured every cm in all holes by core scanning XRF was used to construct a composite section, and low resolution (20 cm) oxygen isotopes of benthic foraminifera were correlated to the marine $\delta^{18}O$ stack of LR04 (Lisiecki and Raymo, 2005) to provide the age model that we present here (Hodell et al., 2015; Hodell et al., 2013) . The record can be correlated unambiguously to the LR04 benthic $\delta^{18}O$ stack, and demonstrates that Site U1385 contains a complete record from the Holocene to 1.43 Ma (Marine Isotope Stage 46). This age model is in general good agreement with the revised position of polarity reversal boundaries and, in particular with the Brunhes-Matuyama transition that occurred at the beginning of MIS 19, ~779 ka, (Hodell et al., 2015) . The age model of this interglacial is based on five control points (Table 1).

2.3 Pollen, geochemical and time-series analyses

2.3.1 Pollen-derived vegetation and climate reconstruction

Sediment subsamples of 1-cm thickness and 2.5-5 cm^3 volume were prepared for pollen analysis using the standard protocol for marine samples, http://www.ephe-paleoclimat.com/Files/Other/Pollen%20extraction%20protocol.pdfhttp://www.ephe-paleoclimat.com/Files/Other/Pollen%20extraction%20protocol.pdf, employing coarse-sieving at 150 µm, successive treatments with cold HCl, cold HF at increasing strength and micro-sieving (10 µm mesh). Known quantities of *Lycopodium* spores in tablet form were added to permit the calculation of pollen concentrations. Slides were prepared using a mobile mounting medium to permit rotation of the grains and counted using a Primo Star light microscope at 400× and 1000× magnifications for routine identification of pollen and spores, respectively. Eighty six samples were analyzed every 2 to 4 cm (450-year average temporal resolution). Pollen counts oscillate between 100 and 144 terrestrial pollen grains excluding *Pinus*, aquatics and spores (total sporo-pollen sum between 168 and 937). The number of morphotypes in most of the samples, 63 out from 86, ranges from 20 to 31, and from 14 to19 in the remaining samples. Pollen percentages for terrestrial taxa were calculated against the main sum of terrestrial grains, while percentages for *Pinus* were calculated against the main sum plus *Pinus*. Aquatic pollen and spores percentages are based on the total sum (Pollen + spores + indeterminables + unknowns). The interpretation of the pollen diagram was assisted by the visual identification of pollen zones that was confirmed by a constrained hierarchical cluster analysis based on Euclidean distance between samples (Fig. S1 and Supplementary Information). Analysis was performed in the R environment v. 2.13.2 (R Development Core Team, 2011) using the *chclust* function from package *Rioja* (Juggins, 2009).

2.3.2 Reconstruction of sea surface temperature and freshwater pulses

Sea Surface temperature (SST) was reconstructed using di- and tri-unsaturated alkenones of 37 carbons, which are organic compounds synthetized by marine coccolithophore algae in a temperature related proportion. Alkenones, in particular $C_{37:4}$, can also be used to track episodes of massive cold freshwater input (from iceberg melting or river discharges) which are responsible for decreasing salinities in the surface water masses (Martrat et al., 2007; Rodrigues et al., 2011). Alkenones are part of the Total Lipid Extracted (TLE) fraction which can be removed from 2g of sediment by sonication with dichloromethane and hydrolysed with 6% potassium hydroxide in methanol. After derivatization with bis(trimethylsilyl)trifluoroacetamide, the TLE was identified using Bruker Mass spectrometer detector and quantified with a Varian Gas chromatograph Model 3800 equipped with septum programmable injector and a flame ionization detector with a CPSIL-5 CB column. As gas carrier was used Hydrogen at 2.5ml/min. Alkenone concentrations were determine using n-hexatriacontane as an internal standard**.** The alkenone index Uk'_{37} was calculated based on the di and tri unsaturated ratio (Prahl and Wakeham, 1987), and converted in to temperature values using the global core top calibration of annual SST (Müller et al., 1998). The average temporal resolution between samples is 528 years.

2.3.3 Oxygen and carbon isotopic analyses of deep and surface dwelling foraminifera

Samples for stable isotope analysis were wet sieved at 63μm and dried in an oven at 50°C. Stable isotopes were measured on the planktic foraminifera *Globigerina bulloides* picked from the 250 to 355 μm size fraction and the benthic foraminifer *Cibicidoides wuellerstorfi* from the >212 um fraction. Foraminifer tests were crushed and soaked in a solution of 1% hydrogen peroxide for 30 minutes in individual vials. Acetone was added and the samples placed in an ultra-sonic bath for 10 seconds, after which the liquid was carefully decanted to remove any contaminants. The samples were dried in an oven at 50˚C overnight. Isotopic analyses of the samples were performed using a VG SIRA mass spectrometer with a Multicarb system for samples of >80μg mass. Analytical precision is estimated to be ±0.08‰ for both $\delta^{18}O$ and $\delta^{13}C$. For smaller samples (<80µg), measurements were performed on a Thermo Finnigan MAT253 mass spectrometer fitted with a Kiel device. Analytical precision is estimated to be ±0.08‰ for $\delta^{18}O$ measurements and ±0.06‰ for $\delta^{13}C$ measurements. All isotope measurements were made in the Godwin Laboratory, University of Cambridge and are reported relative to V-PDB.

2.3.4 Identification of climatic cyclicities

We used the REDFIT methodology and software (Schulz and Mudelsee, 2002), a well-known spectral analysis technique to analyse directly unevenly spaced time series under study, without interpolating them. These time series can be analyzed using the existing standard Fourier spectral analysis techniques. Another advantage of REDFIT is that it is able to take into account the red noise background of the paleoclimate data. Additionally, in order to explore potential climate regime shifts of the paleoclimate data under analysis, we have used a change point method (Zeileis et al., 2003; Zeileis et al., 2002), as implemented in the R package *strucchange* (Zeileis A. et al., 2002). This method is able to test multiple structural changes in linear regression models measuring transitions in the mean and assess their statistical significance (Zeileis et al., 2003). This statistical tool identifies the age where there exists a significant structural change in the times series analysed providing the 95% CI (confidence interval) of the change-point.

3. Results and discussion

3.1. Atmospheric and oceanic changes in the southwestern European region during MIS 19

MIS 19 spanned 33,000 years, from 791 to 758 ka, based on the age of the mid-points between the highest and lowest $\delta^{18}O_b$ values at the transitions MIS 20/19 and MIS 19/18. During MIS 19 $\delta^{18}O_b$ values were lower than 3.5‰ (Fig. 2). The mid-points of the MIS 19c/19b and MIS 19b/19a transitions correspond to the timing of significant shifts in the $\delta^{18}O_b$ record, and are dated in our record at 774 and 765 ka, respectively, (Fig. S2a). The age of the MIS 19c/19b boundary coincides with the radiometric age obtained in the Montalbano Jonico section (Bertini et al.). During the entire MIS 19 the Mediterranean forest cover remained relatively well developed for 27,000 yrs, between 787 and 760 ka, indicating that this region was under the influence of the westerlies that provided winter rainfall to forest growth. Two major Mediterranean forest expansions one during MIS 19c and the other overlapping MIS 19b and 19a followed increases in insolation. Both forest cover increases lagged precession minima by 3-4 millennia in line with the lag between precession and the response of sediment lightness estimated close to site U1385 (Hodell et al., 2015) (Fig. 2). A long-term trend of *Pinus* and heathland (Ericaceae) expansion at the expense of the Mediterranean forest reflect a regional cooling (Polunin and Walters, 1985) that may indicate the progressive southward migration of the polar front as the result of the ice accumulation in the northern high latitudes from MIS 19 to 18.

We defined the beginning of the terrestrial interglacial period, which we named the Tajo interglacial, at 787.5 ka based on the sharp development of both *Isoetes* and Mediterranean forest after the short cooling event lasting less than 1,000 years (Fig. 2). Both criteria were used for identifying the beginning of the Iberian Eemian (Sánchez Goñi et al., 1999). The Tajo interglacial ended at 775 ka and lasted ~12,500 years. It was marked by the strongest expansion of Mediterranean taxa *ss,* reflecting a pronounced seasonal climate with dry and hot summers and cool and wet winters (Polunin and Walters, 1985). Both the onset and the end of the Tajo interglacial represent significant changes in vegetation-based atmospheric regimes (Fig. S2c). The onset of this terrestrial interglacial started well after the MIS 20/MIS 19 transition, ~3,500 years, but the end was nearly contemporaneous with the end of MIS 19c (Fig. 2). During MIS 19c alkenone-based SST remain quite stable at around 18°C as do the planktonic foraminifera oxygen isotope ($\delta^{18}O_{p)}$ values associated with the virtual absence of freshwater fluxes on this margin and the progressive increase in the local $\delta^{13}C_b$-based deep water ventilation (Fig. 3). This warm ocean contrasts with the long-term atmospheric cooling in southwestern Iberia and the gradual decrease in insolation.

Superimposed on the long-term trend in forest cover, six major Mediterranean forest contractions (20% in average of change in pollen percentages) with minima at 782, 778, 774, 768, 764 and 759 ka) indicate that MIS 19 was punctuated by millennial-scale climate changes in southwestern Iberia (Fig. 2). These forest contractions were associated with the development of semi-desert vegetation coeval with the reduction of heathlands and *Pinus*, pointing to colder and drier winters. Ericaceae needs at least 4 months of mean temperatures above 10°C while the forest in temperate latitudes requires a longer period of warmth with a growth period of 4–6 months, and cool but mild winter of 3–4 months (Polunin and Walters, 1985). *Pinus* changes are more difficult to explain as this morphotype includes several pine species with different ecological requirements. With the exception of those during MIS 19a these forest contractions were paradoxically associated with *Isoetes* increases (Fig. 2). The development of *Isoetes,* fern ally, marks the humid and warm interglacials of southwestern Iberia but its present-day maximum development is related to periods of flooding alternating with desiccation in winter (Salvo Tierra, 1990). The concomitant increase of semi-desert plants and *Isoetes* during MIS 19c and 19b may indicate intervals when the westerlies were slightly deflected towards the north and their influence in southwestern Iberia was reduced.

At present, changes in the North Atlantic Oscillation (NAO) marked by changes in the intensity and direction of the westerlies has a substantial impact on the vegetation greenness in Europe (Gouveia et al., 2008). In the Iberian Peninsula, the Mediterranean forest development critically depends on the winter temperatures and water availability during the winter season strongly controlled by the NAO. Two stronger sub-orbital Mediterranean forest decreases, with no *Isoetes* development, are observed during MIS 19a likely indicating a still weaker influence of the westerlies. Conversely, zonal westerly winds brought winter moisture in southwestern Iberia and triggered the observed Mediterranean forest expansions.

The repeated meridional shift in the westerlies would imply (Ruddiman and McIntyre, 1984) successive increases of warm and moist air that was transported to the high latitudes of the North Atlantic via the western boundary current of the North Atlantic subtropical gyre. We should therefore expect warm SST in the subtropical and subpolar gyres concomitant with drought and cooler temperatures in southwestern Iberia. Actually, our record shows a clear air-sea decoupling during MIS 19c (Fig. 3a, 3b). A short-lasting decoupling during MIS 19b and MIS 19a, is only observed at the beginning of the atmospheric cold phases, at 765 and 760 ka. Freshwater fluxes recorded in the eastern part of the subtropical gyre (Fig. 3c) were likely responsible for the cold air-sea coupling at the end of these intervals and during that centered at 769 ka. Within the uncertainties of the age models, these intervals are concomitant with IRD deposition at Site U1314 in the subpolar North Atlantic (Alonso-Garcia et al., 2011). Interestingly, the three major atmospheric cooling and drying events during MIS 19c, with minima at 782, 778 and 774 ka, are not associated with freshwater pulses in the subtropical and subpolar gyres indicating that the cause of these events is not primarily related to high latitude ice-sheet dynamics

(Fig. 3). Therefore, their origin could be sought at the low latitudes forced by precession variations (McIntyre and Molfino, 1996).

To test this hypothesis we performed Fourier spectral analysis of the terrestrial and marine records placed on two age models, the LR04 and the astronomical-tuned age models (Table 1), because the identification of any cyclicity is highly age model dependent. The latter is an alternative age model based on previous studies showing that variations in sediment color of southwestern Iberian Margin sediments contain a strongly modulated precession signal over the past 400 kyr (Hodell et al., 2015). A dominant 5000-year cyclicity of changes in the Mediterranean forest cover is identified using both LR04 and orbitally-tuned models with significance at 95% and 75%, respectively (Fig. 4a and S4). We believe that the 5000-year cyclicity is a robust feature of MIS 19. The lower significance of the spectral analysis using the orbitally-tuned age model is certainly due to a lesser constrained chronology only based on three data points between c. 711 and 805 ka defined by low eccentricity and damped precession signal (Hodell et al., 2015) (Table 1). Additionally, we compared our Mediterranean forest pollen record and its 5-kyr bandpass filter output curve with the variations in the largest amplitude of the seasonal cycle reconstructed from the 24-h mean irradiance of the winter and summer solstices and autumn and spring equinoxes at the equator (Berger et al., 2006) (Fig. 5). This comparison shows the good correspondence between the two records although the magnitude of changes is larger during MIS 19ab than during MIS 19c. The strong forest contractions would be explained by the regional SST cooling associated to the freshwater fluxes arriving at the subpolar gyre. This good correspondence gives support to the low latitude origin of the observed repeated shift of the westerlies in southwestern Iberia at 37°N likely related to the fourth harmonic of precession. Changes of yearly solar radiation in the tropics amplify or relax the thermal latitudinal contrast and, therefore, the oceanic and atmospheric circulation. Actually, we also found a similar 5000-year dominant cyclicity in the regional surface and deep ocean conditions (SST, freshwater pulses, $\delta^{18}O_p$, $\delta^{13}C_b$) (Figs 4b-e) in line with the cyclicity found for $\delta^{18}O_b$ in the central part of the North Atlantic (Site U1313) (Ferretti et al., 2015). Our data clearly show for the first time that the climate of MIS 19, marked by weak eccentricity modulation, was punctuated by 5000-year cyclic changes in the direction of the westerlies likely produced by a precessional component of orbital variation. These changes were associated during MIS 19c with repeated decoupling between cold-dry air in southwestern Iberia and a warm subtropical gyre suggesting periods of increased oceanic and atmospheric circulation. Recent climate model simulations suggest that during drought periods in Iberia the zonal moisture transport is less intense on the subtropics while the meridional moisture transport in the North Atlantic is intensified, in accordance with the barotropic structure of geopotential height anomalies (Liberato et al., 2015).

The 5000-year dominant cyclicity found in the southwestern Iberian margin during MIS 19 is also found in the $\delta^{18}O$ record of the northwestern subtropical Atlantic Ocean between 320-870 ka (Billups and Scheinwald, 2014). It can be surprising to observe this 5000 yr cyclicity in the subtropical latitudes as (Berger et al., 2006) predicted a very low amplitude of the 5.5-kyr precession harmonic during MIS 19 and decreases when getting away from the Equator. The oceanic and atmospheric cyclicity observed in the southwestern Iberian margin may reflect temperature changes in the equatorial source region of the subtropical surface waters and oceanic heat transport, which, at subtropical latitudes is almost half of the total northward heat transport (Weirauch et al., 2008).

3.2 Air-sea interactions in southwestern Europe and ice growth at orbital and suborbital time scales

Observational data and climate model simulations have shown that the increase in the thermal gradient of North Atlantic SST enhances the rates of moisture arriving to the northern hemisphere high latitudes leading to ice growth during the MIS 5e/5d and MIS 5/4 transitions (Risebrobakken et al., 2007; Ruddiman and McIntyre, 1984). Recent work has additionally shown that this increase in the latitudinal thermal gradient is associated with a strong warm sea-cold land contrast in the western European margin, above 40°N, at orbital and millennial time scales during MIS5/4, a period characterized by strong changes in insolation and moderate IRD pulses in the central and western North Atlantic (Sanchez Goñi et al., 2013). We report a similar phenomenon during the MIS 19c/19b transition at lower latitudes than 40°N despite the low amplitude change in insolation that characterizes this transition (Fig. 3). At the timing of these successive decouplings we observe repeated increases in the $\delta^{18}O_b$ values (Fig. 2). It is well known that the $\delta^{18}O_b$ variations depend on changes in continental ice volume, local deep-water temperatures and hydrography (Skinner and Shackleton, 2006). Actually, the trend of $\delta^{18}O_b$ record during MIS 19c partly differs to that of the $\delta^{18}O_{seawater}$-based relative sea level change record from the southern hemisphere site ODP 1123 (Elderfield et al., 2012). However, this latter record shows three decreases of sea-level, slowdown of deglaciation, dated at 784, 778 and 775 ka that despite the ±5 kyrs of chronological uncertainties coincide with the timing of our increases in $\delta^{18}O_b$ values (Fig. 3).

We know that MIS 19 is marked by temperatures slightly cooler in Antarctica, by 1-2°C, lower GHC than those of the present interglacial (Jouzel et al., 2007), and $\delta^{18}O_b$ values heavier than the interglacials younger than MIS 11 (Lisiecki and Raymo, 2005) with higher sea levels characterizing most of the interglacials periods after 450 ka (i.e. MIS 5 and MIS 9 but not MIS 7) (Elderfield et al., 2012). MIS 19 is associated with moderate IRD of European-Greenland-Icelandic origin (Hernández-Almeida et al., 2012; Hodell et al., 2008; Naafs et al., 2011) that may suggest a larger Eurasian ice-sheet development in comparison with that developed during interglacials after MIS 16. The relatively high ice volume baseline conditions of MIS 19 likely allowed this interglacial to be more sensitive to higher frequency climate oscillations than interglacials after 400 ka. However, MIS 5, one of the interglacials with largest changes in insolation and highest sea level was marked by ~ 3,000-2,500 year cyclicity, in the atmosphere of southwestern Iberia (Fig. S4). A similar cyclicity is observed during the Holocene (Fig. S4), which contrasts clearly with that of MIS 19 (Fig. 4a) despite the similarity of both interglacials from an astronomical point of view. If the millennial variability plays a major role in the entering in glaciation as suggested by some authors (e.g. (Tzedakis et al., 2004)), the results presented here put into question both the potential good analogy (Herold et al., 2012; Yin and Berger, 2015; Yin and Berger, 2011) and similar duration (Tzedakis et al., 2012) of the two interglacials under natural boundary conditions (e.g. pre-industrial CO_2 concentrations).

4. Conclusions

Data presented here show for the first time that during MIS 19, an interglacial marked by muted insolation changes, 5000-yr cyclicity paced the shifting of the westerlies and the warm sea surface currents likely due to the response of the Earth system to the harmonics of precession. Along with the decrease in boreal summer insolation, repeated periods of intensified northward transport of heat and associated water vapor during MIS 19c slowed down the deglaciation. These periods may also contribute to the substantial ice accumulation at the MIS 19c/b transition that triggered the successive iceberg discharges during MIS 19ab. Superimposed on this precessional cyclicity, freshwater fluxes would have amplified the cooling at regional and global scale and promote additional ice growth leading to glaciation.

Acknowledgements

This research used samples and data collected through the Integrated Ocean Drilling Program (IODP). This work has been funded by WarmClim, a LEFE-INSU IMAGO project. NERC is acknowledged for the chronostratigraphy of Site U1385. We are grateful to A.-L. Daniau, W. Fletcher and G. Sgubin for constructive discussions, L. Devaux for their invaluable technical assistance, and V. Hanquiez for drawing Fig. 1.

Additional information. Supplementary information is available in the online version of the paper.

Data. The data for this work can be found at

References

Alonso-Garcia, M., Sierro, F.J., Kucera, M., Flores, J.A., Cacho, I., Andersen, N., 2011. Ocean circulation, ice sheet growth and interhemispheric coupling of millennial climate variability during the mid-Pleistocene (ca 800–400 ka). Quaternary Science Reviews, 30, 3234-3247.

Berger, A., Loutre, M.F., 1991. Insolation values for the climate of the last 10 million years. Quaternary Science Reviews, 10, 297-317.

Berger, A., Loutre, M.F., Mélice, J.L., 2006. Equatorial insolation: from precession harmonics to eccentricity frequencies. Climate of the Past, 2, 131-136.

Bertini, A., Toti, F., Marino, M., Ciaranfi, N., 2015. Vegetation and climate across the Early–Middle Pleistocene transition at Montalbano Jonico, southern Italy. Quaternary International, 383, 104-115.

Billups, K., Scheinwald, A., 2014. Origin of millennial-scale climate signals in the subtropical North Atlantic. Paleoceanography, 29, 612–627, doi:10.1002/2014PA002641.

Blanco Castro, E., Casado González, M.A., Costa Tenorio, M., Escribano Bombín, R., García Antón, M., Génova Fuster, M., Gómez Manzaneque, F., Moreno Sáiz, J.C., Morla Juaristi, C., Regato Pajares, P., Sáiz Ollero, H., 1997. Los bosques ibéricos: Barcelona, Planeta, 572 p.

Chapman, M.R., Maslin, M.A., 1999. Low-latitude forcing of meridional temperature and salinity gradients in the subpolar North Atlantic and the growth of glacial ice sheets. Geology, 27, 875-878.

Elderfield, H., Ferretti, P., Greaves, M., Crowhurst, S., McCave, I.N., Hodell, D., and Piotrowski, A.M, 2012. Evolution of Ocean Temperature and Ice Volume Through the Mid-Pleistocene Climate Transition. Science, 337, 704-709.

Ferretti, P., Crowhurst, S.J., Naafs, B.D.A., Barbante, C., 2015. The Marine Isotope Stage 19 in the mid-latitude North Atlantic Ocean: astronomical signature and intra-interglacial variability. Quaternary Science Reviews, 108, 95-110.

Fiúza, A.F.d.G., Macedo, M.E.d., Guerreiro, M.R., 1982. Climatological space and time variation of the Portuguese coastal upwelling. Oceanologica Acta, 5, 31-40.

Ganopolski, A., Rahmstorf, S., 2001. Rapid Changes of glacial climate simulated in a coupled climate model. Nature, 409, 153-158.

Gouveia, C., Trigo, R.M., DaCamara, C.C., Libonati, R., Pereira, J.M.C., 2008. The North Atlantic Oscillation and European vegetation dynamics. International Journal of Climatology, 28, 1835-1847.

Hernández-Almeida, I., Sierro, F.J., Cacho, I., Flores, J.A., 2012. Impact of suborbital climate changes in the North Atlantic on ice sheet dynamics at the Mid-Pleistocene Transition. Paleoceanography, 27, PA3214.

Herold, N., Yin, Q.Z., Karami, M.P., Berger, A., 2012. Modelling the climatic diversity of the warm interglacials. Quaternary Science Reviews, 56, 126-141.

Hodell, D.A., Channell, J.E.T., Curtis, J.H., Romero, O.E., Röhl, U., 2008. Onset of “Hudson Strait” Heinrich events in the eastern North Atlantic at the end of the middle Pleistocene transition (~640 ka)? Paleoceanography, 23, PA4218.

Hodell, D. A., Lourens, L., Crowhurst, S., Konijnendijk, T., Tjallingii, R., Jiménez-Espejo, F., Skinner, L., Tzedakis, P.C., Shackleton Site Project Members, 2015. A reference time scale for site U1385 (Shackleton Site) on the Iberian Margin. Global and Planetary Change, 133, 49-64.

Hodell, D.A., Lourens, L., Stow, D.A.V., Hernández-Molina, J., Alvarez Zarikian, C.A., Shackleton Site Project, M., 2013, The "Shackleton Site" (IODP Site U1385) on the Iberian Margin. Sci. Dril., 16, 13-19.

Jouzel, J., Masson-Delmotte, V., Cattani, O., Dreyfus, G., Falourd, S., Hoffmann, G., Minster, B., Nouet, J., Barnola, J.M., Chappellaz, J., Fischer, H., Gallet, J.C., Johnsen, S., Leuenberger, M., Loulergue, L., Luethi, D., Oerter, H., Parrenin, F., Raisbeck, G., Raynaud, D., Schilt, A., Schwander, J., Selmo, E., Souchez, R., Spahni, R., Stauffer, B., Steffensen, J.P., Stenni, B., Stocker, T.F., Tison, J.L., Werner, M., Wolff, E.W., 2007. Orbital and Millennial Antarctic Climate Variability over the Past 800,000 Years. Science, 317, 793-796.

Juggins, S., 2009, Package “rioja” - Analysis of Quaternary Science Data, The Comprehensive R Archive Network.

Liberato, M.L.R., I., M., Russo, A., Gouveia, C., Ramos, A.M., Trigo, R.M., 2015. Widespread extreme drought events in Iberia and their relationship with North Atlantic moisture flux deficit. Geophysical Research Abstracts, 17, EGU2015-6771.

Lisiecki, L., Raymo, M.E., 2005. A Pliocene-Pleistocene stack of 57 globally distributed benthic δ 18 O records. Paleoceanography, 20, PA1003.

Marcott, S.A., Clark, P.U., Padman, L., Klinkhammer, G.P., Springer, S.R., Liu, Z., Otto-Bliesner, B.L., Carlson, A.E., Ungerer, A., Padman, J., He, F., Cheng, J., Schmittner, A., 2011. Ice-shelf collapse from subsurface warming as a trigger for Heinrich events: Proceedings of the National Academy of Sciences, 108, 13415-13419.

Martrat, B., Grimalt, J.O., Shackleton, N.J., De Abreu, L., Hutterli, M.A., Stocker, T.F., 2007. Four cycles of recurring deep and surface water destabilizations on the Iberian margin. Science, 317, 502-507.

McAyeal, D.R., 1993. Binge/purge oscillations of the Laurentide ice sheet as a cause of North Atlantic's Heinrich events. Paleoceanography, 8, 775-784.

McIntyre, A., Molfino, B., 1996. Forcing of Atlantic Equatorial and subpolar millennial cycles by precession. Science, 274, 1867-1870.

Müller, P.J., Kirst, G., Ruhland, G., von Storch, I., Rosell-Melé, A., 1998. Calibration of the alkenone paleotemperature index U37K' based on core-tops from the eastern South Atlantic and the global ocean (60°N-60°S). Geochimica et Cosmochimica Acta, 1757-1772.

Naafs, B.D.A., Hefter, J., Ferretti, P., Stein, R., Haug, G.H., 2011. Sea surface temperatures did not control the first occurrence of Hudson Strait Heinrich Events during MIS 16. Paleoceanography, 26, PA4201.

Naughton, F., Sanchez Goñi, M.F., Desprat, S., Turon, J.-L., Duprat, J., Malaizé, B., Joli, C., Cortijo, E., Drago, T., Freitas, M.C., 2007. Present-day and past (last 25000 years) marine pollen signal off western Iberia. Marine Micropaleontology, 62, 91-114.

Paillard, D., Labeyrie, L., Yiou, P., 1996. Macintosh Program performs time-series analysis. Eos Trans. AGU, 77, 379-379.

Peinado Lorca, M., Martínez-Parras, J.M., 1987. Castilla-La Mancha, In: Peinado Lorca, M., and Rivas Martínez, S., (Eds.) La vegetación de España. Alcala de Henares, Universidad de Alcalá de Henares, p. 163-196.

Polunin, O., Walters, M., 1985. A guide to the vegetation of Britain and Europe. New York, Oxford University Press, 238 p.

Prahl, F.G., Wakeham, S.G., 1987. Calibration of unsaturation patterns in long-chain ketone compositions for palaeotemperature assessment. Nature, 330, 367-369.

R Development Core Team, 2011, R: A language and environment for statistical computing: Vienna, Austria, R Foundation for Statistical Computing.

Ríos, A.F., Pérez, F.F., Fraga, F., 1992. Water masses in the upper and middle North Atlantic Ocean east of the Azores: Deep Sea Research Part A. Oceanographic Research Papers, 39, 645-658.

Risebrobakken, B., Dokken, T., Ottera, O.H., Jansen, E., Gao, Y., Drange, H., 2007. Inception of the Northern European ice shet due to contrasting ocean and insolation forcing. Quaternary Research, 67, 128-135.

Rodrigues, T., Voelker, A.H.L., Grimalt, J.O., Abrantes, F., Naughton, F., 2011. Iberian Margin sea surface temperature during MIS 15 to 9 (580–300 ka): Glacial suborbital variability versus interglacial stability. Paleoceanography, 26, PA1204.

Ruddiman, W.F., McIntyre, A., 1984. Ice-age thermal response and climatic role of the surface Atlantic Ocean, 40°N to 63°N. Geological Society of America Bulletin, 95, 381-396.

Salvo Tierra, E., 1990. Guía de helechos de la Península Ibérica y Baleares: Madrid.

Sanchez Goñi, M.F., Bard, E., Landais, A., Rossignol, L., d'Errico, F., 2013. Air-sea temperature decoupling in western Europe during the last interglacial-glacial transition. Nature Geoscience, 6, 837-841.

Sánchez Goñi, M.F., Eynaud, F., Turon, J.-L., Shackleton, N.J., 1999. High resolution palynological record off the Iberian margin: direct land-sea correlation for the Last Interglacial complex. Earth and Planetary Science Letters, 171, 123-137.

Schulz, M., Mudelsee, M., 2002. REDFIT: estimating red-noise spectra directly from unevenly spaced paleoclimatic time series. : Computers & Geosciences, 28, 421-426.

Shackleton, N.J., Hall, M.A., Vincent, E., 2000, Phase relationships between millenial scale events 64,000-24,000 years ago. Paleoceanography, 15, 565-569.

Short, D.A., Mengel, J.D., Crowley, T.J., Hyde, W.T., North, G.R., 1991. Filtering of Milankovitch cycles by Earth's geography. Quaternary Research, 35, 157-173.

Skinner, L.C., Shackleton, N.J., 2006, Deconstructing Terminations I and II: revisiting the glacioeustatic paradigm based on deep-water temperature estimates. Quaternary Science Reviews, 25, 3312-3321.

Stow, D.A.V., Hernández-Molina, F.J., Alvarez Zarikian, C.A., the Expedition 339 Scientists, 2013, Proceedings IODP, 339, Tokyo (Integrated Ocean Drilling Program Management International, Inc.).

Tuenter, E., Weber, S.L., Hilgen, F.J., Lourens, L.J., 2007. Simulating sub-Milankovitch climate variations associated with vegetation dynamics. Climate of the Past, 3, 169-180.

Tzedakis, P.C., Channell, J.E.T., Hodell, D.A., Kleiven, H.F., Skinner, L.C., 2012. Determining the natural length of the current interglacial. Nature Geoscience, 5, 138–141.

Tzedakis, P.C., Roucoux, K.H., de Abreu, L., Shackleton, N.J., 2004. The duration of forest stages in southern Europe and interglacial climate variability. Science, DOI:10.1126/science.1102398.

Weirauch, D., Billups, K., Martin, P., 2008. Evolution of millennial-scale climate variability during the mid-Pleistocene. Paleoceanography, 23, PA3216.

Yin, Q., Berger, A.. 2015. Interglacial analogues of the Holocene and its natural near future. Quaternary Science Reviews, 120, 28-46.

Yin, Q.Z., Berger, A., 2012. Individual contribution of insolation and CO2 to the interglacial climates of the past 800,000 years. Climate Dynamics, 38, 709-734.

Zeileis, A., Kleiber, C., Krämer, W., Hornik, K., 2003. Testing and dating of structural changes in practice: Computational Statistics & Data Analysis, 44, 109-123.

Zeileis A., Leisch, F., Hornik, K., Kleiber, C., 2002. Strucchange: an R package for testing for structural change in linear regression models: Journal of statistical software, 7, 1-38.

Table legends

Table 1 – Control points used for the two age models of the MIS 19 interval of Site U1385 (Hodell et al., 2015) discussed in the text.

Figure Legends

Figure 1 – Location of the sites discussed in the text. SPG: Subpolar gyre, NAC: North Atlantic Current, AC: Azores Current, STG: Subtropical Gyre, CC: Canary Current, PC: Portugal Current, MJS: Montalbano Jonico Sequence.

Figure 2 – Vegetation changes versus the $\delta^{18}O_b$ record from Site U1385 for MIS 19. **a-f**, Percentages of *Isoetes* spores (cyan) and of semi-desert pollen (*Ephedra distachya*-type, *E. fragilis*-type, Chenopodiaceae, *Artemisia*) in orange (**a**), pollen percentages of the Mediterranean taxa (evergreen *Quercus, Olea, Pistacia, Phillyrea, Cistus*) in red and

Mediterranan forest in light green (mainly deciduous *Quercus*, and Mediterranean taxa). Dark green curve: 3-point weigthed-average smoothing (**b**), pollen percentages of heathlands (Ericaceae) (**c**), pollen percentages of *Pinus* (**d**), $\delta^{18}O$ record from benthic foraminifer ($\delta^{18}O_b$) *Cibicidoides wuellerstorfi,* Black curve: 3-point weigthed-average smoothing (**e**), changes in insolation at 65°N in July (in black), in the precession index (e*sinω) (in red) and obliquity (light blue) (Berger and Loutre, 1991) (**f**). MIS: Marine Isotopic Stage. Orange and grey vertical panels indicate the Tajo interglacial and the MIS 19b, respectively. Black arrows indicate Mediterranean forest contractions; Blue arrow indicate the 1000-yr long lasting cooling event before the onset of the Tajo interglacial.

Figure 3 – Direct comparison between atmospheric conditions in southwestern Iberia and deep and surface oceanic conditions in the eastern subtropical gyre from Site U1385 versus changes in the subpolar gyre from site U1314 for MIS 19. **a-f** pollen percentages of Mediterranean forest (green) (**a**), UK'_{37}-based SST record (purple) and foraminifera-based SST record from the subpolar gyre (black), IODP 1314 (Alonso-Garcia et al., 2011) (**b**), $C_{37:4}$-based freshwater pulse record (purple) and Ice Rafted Debris (IRD) concentration record from U1314 (black) (Alonso-Garcia et al., 2011) (**c**), $\delta^{13}C_b$ record of *Cibicidoides wuellerstorfi* (**d**), e) $\delta^{18}O_p$ record of *Globigerina bulloides*, $\delta^{18}O_{seawater}$-based sea level relative changes (Elderfield et al., 2012) (**f**). Grey bands correspond to the major contractions of the Mediterranean forest associated with full or partial SST warmth and $\delta^{13}C_b$ (deep water ventilation) increase.

Fig. 4 – REDFIT spectral analysis (smoothed Lomb-Scargle peridogram with 6 degree of freedom) of the vegetation-derived atmospheric changes and deep and surface oceanic conditions in southwestern Iberia and its margin for MIS 19. **a-f**. Mediterranean forest (**a**),

$\delta^{18}O_p$ of *G. bulloides* (**b**), C37:4-based freshwater pulses (**c**), alkenone-based SST (**d**), $\delta^{13}C_b$ of *C. wuellerstorfi* (**e**) and $\delta^{18}O_b$ of *C. wuellerstorfi* (**f**).

Figure 5 – Changes in the Mediterranean forest pollen percentages (original data, light green, and 3-point weigthed-average smoothed data, dark green) and its 5-kyr bandpass filter (bandwith of 0.02 on the original data, Analyseries, (Paillard et al., 1996)) (**a, b**) compared with the largest amplitude of the seasonal cycle at the equator (**c**) and the precession index ($e^*\sin\omega$) (in red) (Berger and Loutre, 1991) (**d**).

Figure 1

Click here to download Figure: Fig 1 MapNew.pdf

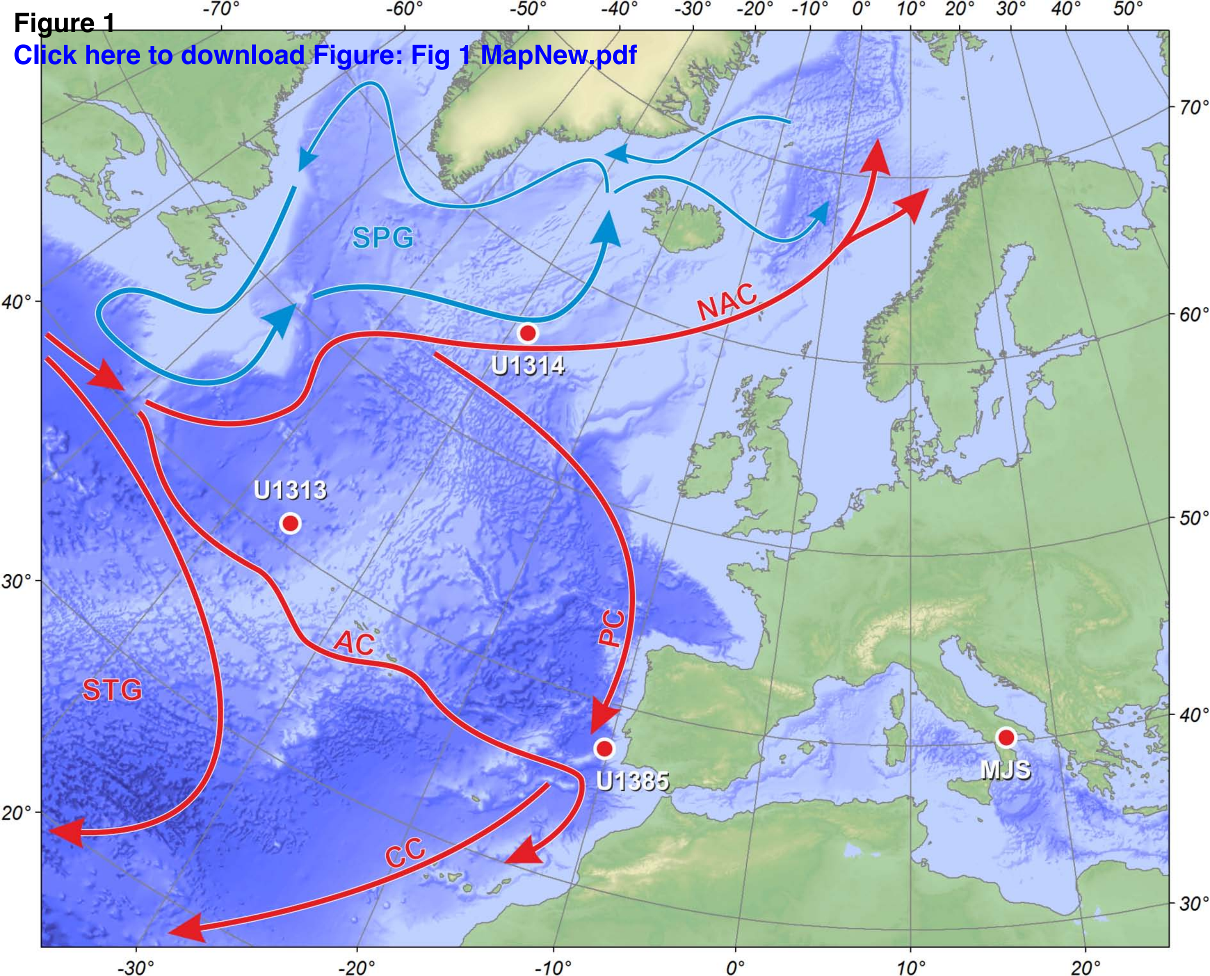

Figure 2

Click here to download Figure: Fig 2(2)_MIS19_pollen4_age.pdf

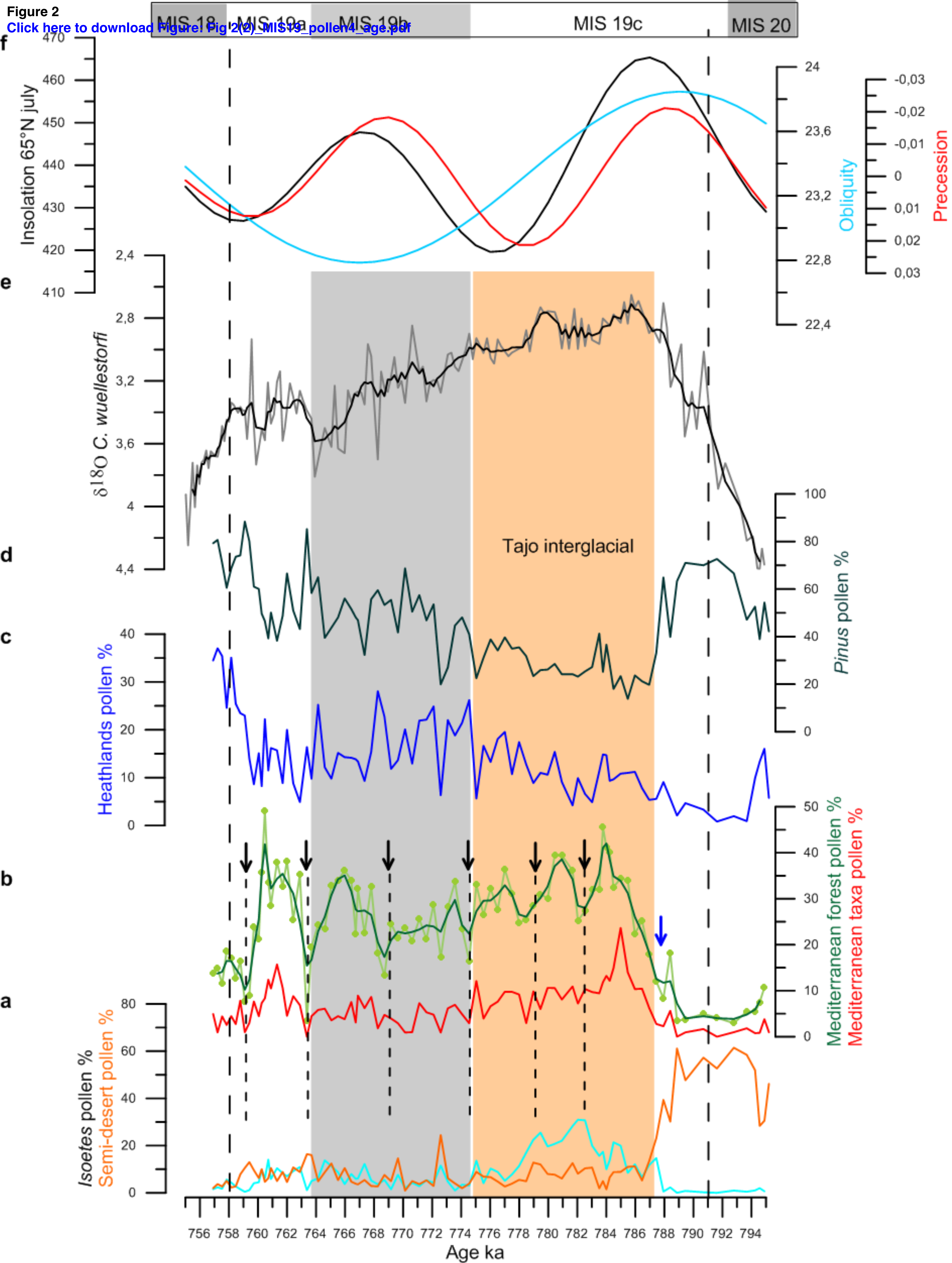

Figure 3
Click here to download Figure: Fig 3(2)_Multiproxy(3)_U1385_U1314_MIS19.pdf

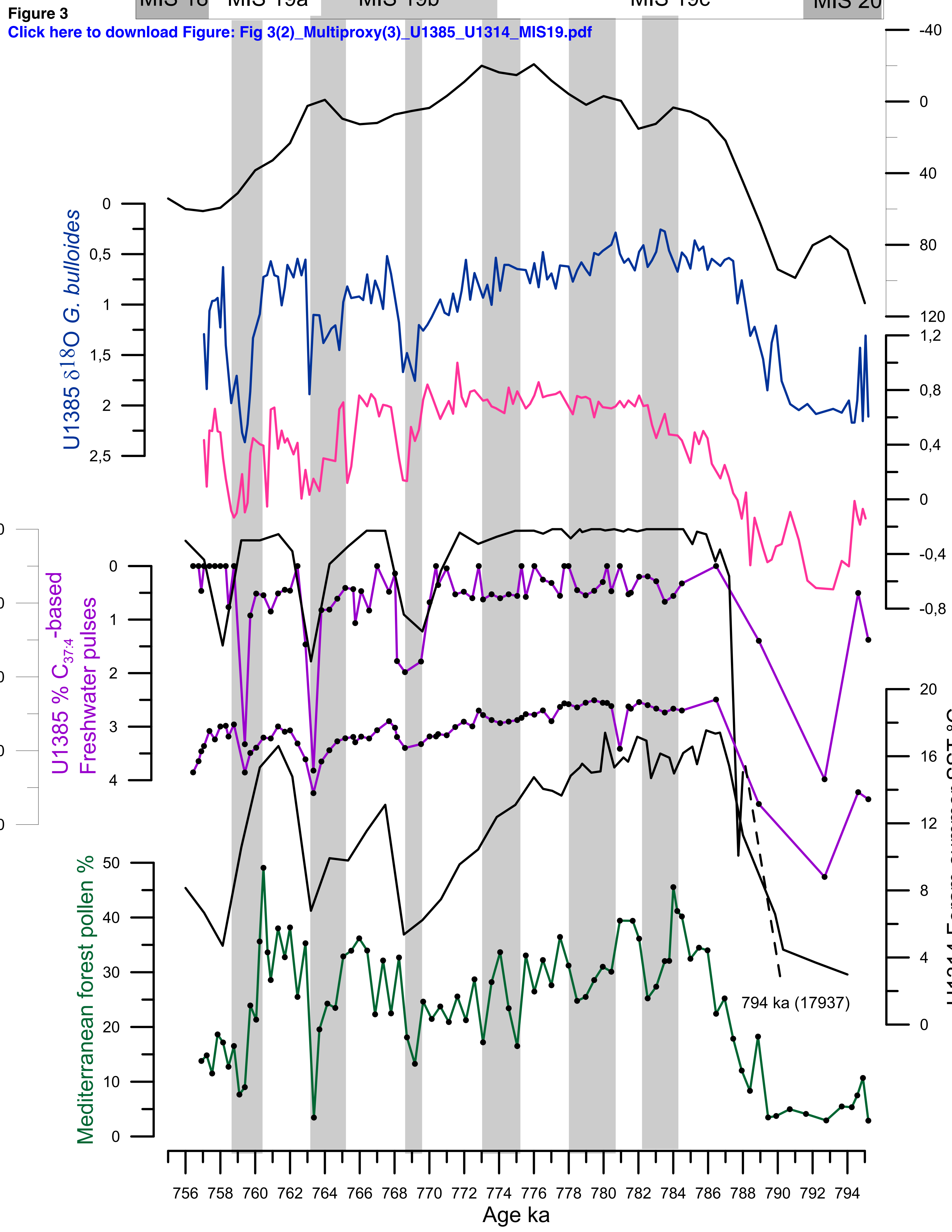

Figure 4

Click here to download Figure: Fig 4_REDFIT_ver25a

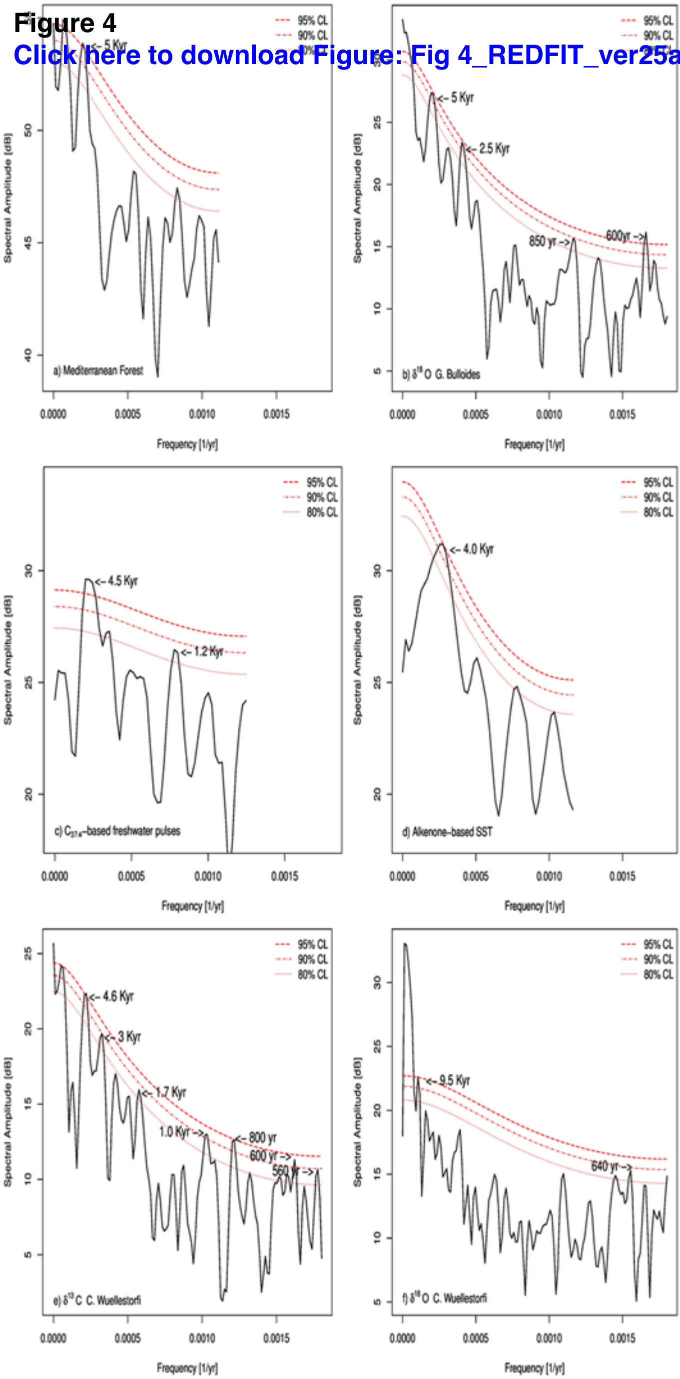

Figure 5

Click here to download Figure: Fig 5_MIS19_pollen4_age_Precession(2

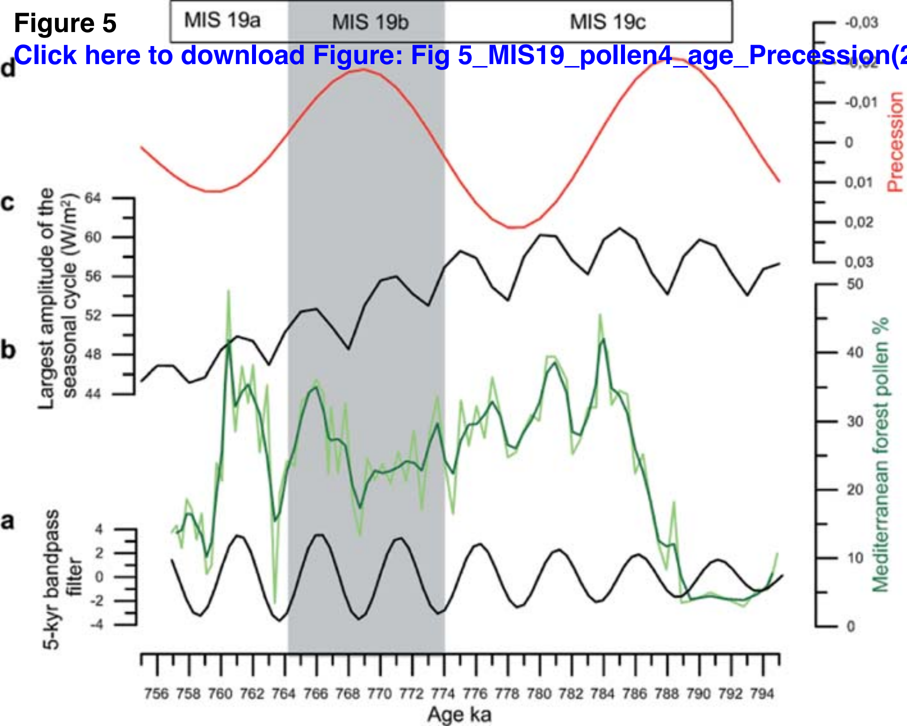

Figure 1 (high-resolution)
Click here to download Figure (high-resolution): Fig 1(high resolution) MapNew.png

Figure 2 (high-resolution)
Click here to download Figure (high-resolution): Fig 2(high resolution)_MIS19_pollen4_age.eps

Figure 3 (high-resolution)
Click here to download Figure (high-resolution): Fig 3(high resolution)_Multiproxy(3)_U1385_U1314_MIS19.eps

Figure 4 (high-resolution)
Click here to download Figure (high-resolution): Fig 4(high resolution)_REDFIT_ver25ago2015.eps

Figure 5 (high-resolution)
Click here to download Figure (high-resolution): Fig 5(high resolution)_MIS19_pollen4_age_Precession(2).eps

Table1

Click here to download Table: Table 1.xlsx

Site U1385	LR04	Site U1385	Astronomically-tuned
Depth (crmcd)	Age (ka)	Depth (crmcd)	Age (ka)
86.944	740.67	83.292	711.86
89.756	762.05	91.447	785.72
92.173	790.06	93.249	804.93
92.344	794.04		
95.654	820.57		